Comparison of γ-ray spectrometry and ICP-MS methods for measuring heat-producing radioactive elements of rocks: a case study on borehole samples from the Sichuan basin, China

Chuanqing Zhu*[1, 2] Ming Xu[3] Nansheng Qiu[1] Shengbiao Hu[4]

[1] *State Key Laboratory of Petroleum Resources and Prospecting, China University of Petroleum, Beijing 102249, China*

[2] *School of Geographical and Earth Sciences, University of Glasgow, Glasgow G12 8QQ, UK*

[3] *Tianjin Geothermal Exploration and Development-design Institute, Tianjin 300250, China*

[4] *State Key Laboratory of Lithospheric Evolution, Institute of Geology and Geophysics, Chinese Academy of Sciences, Beijing 100029, China*

*Corresponding author

Mobile: + 44- 07783838861

E-mail: zhucq@cup.edu.cn; chuanqing.zhu@glasgow.ac.uk

Abbreviated title: Comparison of different methods for measuring heat-producing radioactive elements

Abstract: We compared the consistency of γ-ray spectrometry and inductively coupled plasma mass spectrometry (ICP-MS) by analyzing measurement results of the radioactive heat-producing elements U, Th, and K from borehole samples. This analysis was based on 49 samples obtained from mudstone, siltstone, and carbonate rock, and 11 of the 15 control groups showed great consistency. The radioactive heat production(RHP) of carbonate rocks was relatively low (0.23-0.63 μW m^{-3}) and was mainly contributed by U. Mudstone and siltstone have higher RHPs, which was 1.73 ± 0.46 μW m^{-3} and 2.04 ± 0.49 μW m^{-3}, respectively.

Keywords: γ-ray spectrometry; ICP-MS; Radioactive heat production; Radioactive elements; Sichuan basin

Introduction

Heat production rate of rocks is an important and essential parameter for studies on terrestrial heat flow, deep thermal conditions and lithospheric thermal structure. It is also essential for the research on the thermal history of basins. Acquisition of accurate rock heat-production data is of great significance for studies involving present- and paleo-geothermal field calculations [1, 2], continental lithosphere structure [3-7], tectonic activity and lithospheric evolution [8, 9] and thermal evolution simulation of hydrocarbon source rocks and oil and gas resource assessment. The earth crust contains over 60 unstable nuclides, among which three elements (uranium, thorium, and potassium) can provide large amounts of thermal energy from radioactive isotopes. The temporal and spatial distributions of radioactive elements have great influences on the earth internal thermal field and their contribution to the earth surface heat flow can exceed 30-40% [7, 10, 11].

The heat production rate of crustal rocks is primarily determined by the geochemical method, which involves directly measuring the content of the radioactive heat-producing elements U, Th, and K in rock samples. Compared with the seismic wave speed method and geophysical logging method, the geochemical method produces higher quality data and is now the most common method used to determine the heat production rate of rocks. Currently, the primary methods for measuring the radioactive heat-producing element content are inductively coupled plasma mass spectrometry (ICP-MS) [12] and γ-ray spectrometry [13-21]. This paper analysed the differences between the two, based on measurement results obtained from sedimentary basin borehole core samples.

Geological background and sample preparation

Geological background

The diamond-shaped Sichuan Basin, located in southwest China, is surrounded by mountain ranges (Fig. 1a). The Sichuan Basin began to develop at the base of the Upper Yangtze Platform and has undergone two evolutionary stages: an oceanic cratonic basin stage and a continental foreland basin stage. The end of the Middle Triassic was the Upper Yangtze region’s oceanic-continental sediment convergence period. Before this, the deposits of this region consisted primarily of marine carbonate rocks, sandstones and mudstones. After this period, the deposits consisted primarily of clastic sedimentary rocks (Fig. 1b). During the Cambrian to Early Ordovician, which was a period of cratonic

basin subsidence, marine transgressive sand-shale deposits began forming, with carbonate rocks and evaporites towards the top. Then the Yangtze Plate converged with the Cathaysian Block in the Middle Ordovician, resulting in the basin's uplifting. The basin's Central Uplift expanded in the Silurian, and sandy shale with limestone intercalation deposits as well as sheet stone deposits developed at the edge of the craton, causing the Silurian, Devonian, and Carboniferous to disappear in the basin.

The Permian formed on top of the Carboniferous. Carbonate rocks and evaporites formed during the Early and Middle Triassic, and the Feixianguan Formation developed on top of the Permian. The Sichuan Basin went through a marine-continental transition period during the Late Triassic, and the deposits transformed from marine carbonate-evaporite rock to continental fluvial-deltaic deposits. The Jurassic was characterized by the red clastic rock deposits and lacustrine carbonate at the center of the lake. Then the lake basin shrank in the Cretaceous Period, occupying mainly southern and western Sichuan, and contained sandstone and mudstone deposits.

Sample preparation

The borehole samples were collected from the drill cores in the subsurface strata. These drill cores are marked with depth and their startigraphical properties can be judged by geophysical prospecting and well logging. Therefore, the borehole sample is the most direct approach to study the earth interior. It is frequently used in mineral exploration and geological research. A data column can be set up based on the analysis result of the borehole samples.

The samples in this study come from boreholes in the Sichuan basin, with the exception of boreholes KQ3 and HC1 (located at the edge of the present basin area), and consist mainly of mudstones, sandstones, siltstones, and carbonate rocks (Fig. 1b). The samples were pulverized by the self-developed rock crushers in the State Key Laboratory of Lithospheric Evolution, Institute of Geology and Geophysics, Chinese Academy of Sciences.

Experimental Procedure

Calculation method of the heat production rate

During heat production rate measurements, the content of U, Th, and K in the rock samples is determined and the radioactive heat production(RHP) can be calculated with

empirical formulas. Although many formulas had been presented in recent years [22-24], the coefficients from Rybach (1988) [25] are the most used in literature[26]:

$$A = \rho\,(9.52\,C_U + 2.56\,C_{Th} + 3.48\,C_K)\,10^{-5} \qquad (1)$$

where A is the rock's radioactive heat production (in $\mu W\ m^{-3}$), ρ is the rock density (in $kg\ m^{-3}$), and C_U, C_{Th}, and C_K represent the rock's U (in $\mu g\ g^{-1}$), Th (in $\mu g\ g^{-1}$), and K (in weight%) contents, respectively.

Experimental approaches

We have two groups of samples which are labeled as "S" and "C". Each sample in both groups is also labeled with a number. The samples who have the same number are considered as the same sample because they were collected from the same lithological section in the same strata of a borehole. The comparison used in this study intentionally incorporates conditions that could produce inconsistent results. For example, while the compared samples came from the same boreholes and had identical stratigraphy and lithology, the sampling depths were not entirely consistent (Table 1). If the measurement results are still identical, this proves not only the comparability between the two methods but also the consistency in content of the radioactive heat-producing elements with the same lithology and from the same stratigraphy.

S-samples (measured using the ICP-MS methods) were dissolved by the mixed acid closed digestion method. ^{238}U and ^{232}Th were measured by PerkinElmer, Type Elan DCR-e ICP-MS, using the standard mode (neither KED nor DRC mode was used), while ^{40}K was measured by PerkinElmer Type 5300DV ICP-OES, under conditions of 20 ℃ and relative humidity of 30%. The dilution factor was 500 (dilute 0.1g to a constant volume of 50 ml). The experiment was conducted according to the QC reference material GBW07106. The blank values of both U and Th were adopted as 0.003ng/ml. The Relative Standard Deviation(RSD) of the measured data was estimated as: RSD<5%, while the concentration > 1ppm; RSD<10%, while the concentration < 1ppm.

The other set of samples (labelled C-samples, measured by γ-ray spectroscopy method) were analyzed at the Lab of Cosmogenic Nuclide Chronology, Institute of Geology and Geophysics, Chinese Academy of Sciences, using a hyper-pure γ-ray detector (HPGe) with an efficiency of around 30%. Each sample was measured during an accumulating time of 24 h. An empty cylindrical plastic container was placed in the

detection system for a counting period of 24 h, in order to collect the background count rates. The naturally occurring radionuclides considered in the present analysis of the measured γ-ray spectra are: ^{212}Pb (with a main gamma energy at 239 keV and a gamma yield of 43.1%), ^{214}Pb (352 keV, 37.1%), ^{214}Bi (609 keV, 46.1%), ^{228}Ac (911 keV, 29.0%) and ^{40}K (1461 keV, 10.7%). Under the assumption that secular equilibrium was reached between ^{232}Th and ^{238}U and their decay products, the concentration of ^{232}Th was determined from the average concentrations of ^{212}Pb and ^{228}Ac in the samples, and that of ^{238}U was determined from the average concentrations of the ^{214}Pb and ^{214}Bi decay productsm[15, 21]. As a result, the radionuclide concentrations of ^{232}Th and ^{238}U were obtained. ^{40}K concentration was achieved through a direct measurement. The systems calibration was performed by using a reference material of GBW08304. When sampling ^{137}Cs, ^{210}Pb, ^{226}Ra, ^{238}U, ^{232}Th, and ^{40}K nuclides with this spectrometer for 24 h, the confidence level exceeds 99%, meaning that the gross counts > $3C_{BK}^{1/2}$ (C_{BK} indicates background counts) and the minimum detectable activities are 0.5, 3.3, 0.85, 4.0, 0.45, and 7.0 dpm, respectively. Details of energy and efficiency calibration methods, and quality control follow the method described by Foster et al [20]. In addition, the precise experiment of this method is not the major motivation for the ICP-MS measurements. We focused on examining the uniformity for the same samples (samples collected from the same lithological section of the drill cores) and this work was not limited in comparison of the precisions of the two methods.

Results and discussion

Table 2 and Table 3 show the measurement results. The sample data are divided into three stages for comparison. The direct measurement results of individual samples are presents in the first stage. The second stage consists of samples taken from identical boreholes and having identical stratigraphy and lithology (divided into S-group and C-group based on their measurement method). In the third stage, we consider the S-samples and C-samples that taken from identical boreholes and having identical stratigraphy and lithology as one group. The standard deviation have not been given for the A_S or A_C data in the third stage, because some of them were calculated from multi- individual measurement results but the other ones used the measurement results directly.

Figure 2 shows that 11 out of the 15 sample groups, with the exception of C1, C7, C12, and C14, have similar heat production rate values. It is hard to determine the reason behind the larger discrepancies in the sample testing results, however, since 73.3% of the sample heat production rate values fall within a range that allows for their comparison. Therefore, our preliminary conclusion is that the results obtained using the two testing methods can be used as the basis for further analysis. In order to facilitate comparison, we selected the 11 sets of C and S samples with relatively close thermal conductivity and calculated their average values. Figure 3 shows the averaged heat production rate values for the most similar samples. The margin of error between the C and S samples fell between 0.4% (S5: 1.96 μW m^{-3}; C5: 1.95 μW m^{-3}) and 18% (S10: 2.13 μW m^{-3}; C10: 2.60 μW m^{-3}), except for the No.11 group, for which the difference reached 38%, due to the very low values (S11: 0.17 μW m^{-3}; C11: 0.23 μW m^{-3}) with greater uncertainties.

When taking into account sample lithology, the heat production rate values vary greatly with different lithologies, ranging from 1.73 ± 0.46 μW m^{-3} for siltstone (G2, G8), 2.04 ± 0.49 μW m^{-3} for mudstone (G3, G4, G5, G9, and G10), and 0.50 ± 0.12 μW m^{-3} for dolomite. The statistical results conform to the general relationship between heat production rates and lithology, meaning that carbonate rocks have a lower heat production rate than clastic rocks. In addition, the heat generation rate of the Triassic mudstone samples (G3, G4, and G5) from the HC1 borehole is lower than that of the Paleozoic mudstone samples (G9, G10) from the KQ3 borehole, which is a reflection of the regional and stratigraphic differences.

In general, the Upper Yangtze region, especially the inner Sichuan Basin, has a relatively low heat production rate. For example, the Qaidam Basin on the west side of the Qinghai-Tibetan plateau reaches an average heat production rate of 2.0-2.2 μW m^{-3} [27]. However, the Sichuan Basin is a foreland basin that began to form on top of the ancient cratonic basement during the final phase of the Middle Triassic, and the Emeishan basalts eruption during the Late Permian formed the distinctive Large Igneous Province on the outer rim of the basin. The relatively low heat production rates of ancient carbonate rocks and basaltic rocks (~0.11 μW m^{-3}; 0.63 ± 0.12 μW m^{-3}) [16, 28] may be one of the reasons why the rock formations of the Paleozoic and basaltic provenance areas of the Sichuan Basin have relatively low heat production rates.

Figure 4 shows the heat contribution of heat-generating elements. It is evident that both measurement methods produce highly consistent results, showing that, in general, U and Th have greater contributions and K has a lower contribution. Samples S13 and C13 show a discrepancy in heat-contributing elements; in the former, U has the highest contribution rate, whereas in the latter, Th and K contribute more. The lithology of this sample group was algal dolomite, and so it can be inferred that during sample processing, the main contributing source in S13 was marine sedimentss, in which U is often the dominant contributor (97%, [29]), whereas the main contributing source in C13 was algae. Naturally, the heat generation rate of the rock and the contribution of the heat production rate of each element varies in different regions. For example, in some regions in Egypt, the contribution of the heat production rate of U in metamorphic rocks and pyrogenic rocks can reach up to 51-76% [16], whereas the contribution of the heat production rate of U in sedimentary rocks is 62-69.6%, as compared to 26.9-34% in Th and less than 5% in K [30]. However, in the Alps-Apennines boundary zone, potassium contributes to heat generation on average by 17% [29]. It can be also realized that the results of the contribution rate of the three radioactive element were very uniform ($|D|<0.3$), while the RHPs were greater than 1.0 $\mu W\ m^{-3}$.

In Fig. 5, it can be seen that samples with different lithologies differ more from each other, while samples with the same lithology are consistent. Dolomites (C12, C15, and S13) are mainly gathered in region A, where the contribution rate of U ranges from 82.5% (S15) to ~100% (C12)， while the contribution rate of Th is < 13%. Mudstone (C3, C4, C5, C7, C9, and C10) is mainly gathered in region B, where the contribution of U is < 40%, while the contribution of Th is > 45%. The distribution of siltstone (region C) is closer to mudstone, and forms a transitional distribution from region A to nearby region B. Compared with mudstones, the contribution of U in siltstone is greater, while the contribution of Th is smaller, as shown in Fig. 6. We calculated the average contribution of the heat production rate of U and Th as 50% and 47% in mudstones respectively, and that of the heat production rate of U and Th as 47.4% and 41.6% in siltstones respectively.

The vertical distribution of U, Th, and K and of the element ratios (U/K, U/Th, and Th/K) reflects the sedimentation environment and history [19, 31-34]. In this study, the ratio of U/Th is 0.20 in mudstone and 0.30 in siltstone, possibly due to the fact that

uranium migrates easily into the external environment, and compared with siltstone deposits, mudstone deposits are more susceptible to damage due to exhaustive weathering.

The distribution of radiogenic heat production in the continental lithosphere is very important to geothermic and lithospheric studies. But continental crust rocks show a high variability in radiogenic heat production (RHP) due to their petrogenesis and the complex differentiation and redistribution processes affecting the whole lithosphere. The trace element character of U and Th and their association with accessory minerals makes it difficult to establish a direct relationship between RHP and lithology. These factors impede any efforts to find a simple depth-dependent function for RHP within the continental crust [35]. However, the measurement of the samples from the boreholes made it possible to observe the distribution of the heat production in the upper crust in the research area. With the using of the heat production rate dataset, the heat flow contribution of the upper crust can be estimated, and the lithospheric thermal structure can also revealed.

K has a relatively low heat production contribution, which is negligible for heat production rate calculations in the shallow parts of the earth's crust [16]. However, in deeper parts of the earth, including the core, K is assumed to be an important heat-producing element [36]; therefore, the surface heat flow, which also includes mantle heat currents, contains the heat produced by K in the deeper parts of the earth.

Conclusions

The following conclusions were obtained through the comparison of the γ-ray spectrometry and the ICP-MS radioactive nuclide measurement results and the heat production rate result analysis.

Other than the measurement differences caused by the lithological changes, most of the compared samples had consistent radioactive nuclide content values and heat production rate calculation results, demonstrating that both methods of measuring radioactive nuclides (γ-ray spectrometry and ICP-MS) are highly stable. The result provide a reference for the uniformity between the two experimental methods of rock sample analysis. It also proved the rationality of the integrate use for the heat production rate data that analysed by the two different methods.

The rock heat production rate and the contribution of the heat production rate of each heat-producing element are primarily related to lithology. Carbonate rock, especially dolomite, has a lower heat production rate, ranging from 0.23-0.63 $\mu W\ m^{-3}$, with U being the primary contributor and the other two heat-producing elements having smaller contributions. Mudstone and siltstone have higher heat production rates, $1.73 \pm 0.46\ \mu W\ m^{-3}$ and $2.04 \pm 0.49\ \mu W\ m^{-3}$, respectively, with U and Th being the primary contributors. In mudstone, thorium's contribution rate (50.0%) is greater than uranium's (47.0%), while in siltstone, uranium's rate (47.4%) is greater than thorium's (41.6%).

Acknowledgements

The study was supported by the National Science Foundation of China (Grant No. 41690133, 41772248), the "National Science and Technology Major Project" of China (Grant No. 2017ZX05008004) and the Beijing Training Project of Science and Technology Nova and Leading Talent (Grant No. Z171100001117163). The first author is grateful to the Chinese Scholarship Council (CSC) for supporting him stay in the University of Glasgow as a sponsored researcher. We thank Dr. Bing Xu and Mu Liu for their help in the sample analysis and the reviewers for their constructive suggestions, which clarified many points of this article.

Figures

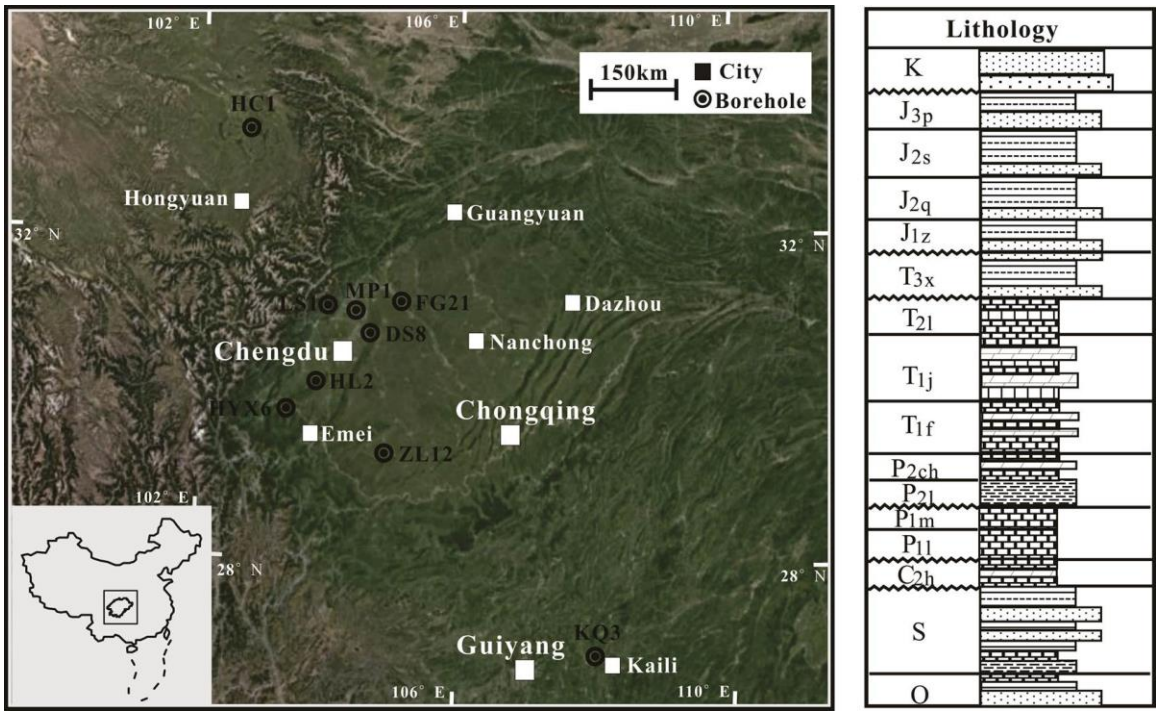

Fig. 1 Sampling borehole locations and stratigraphic column of the research area

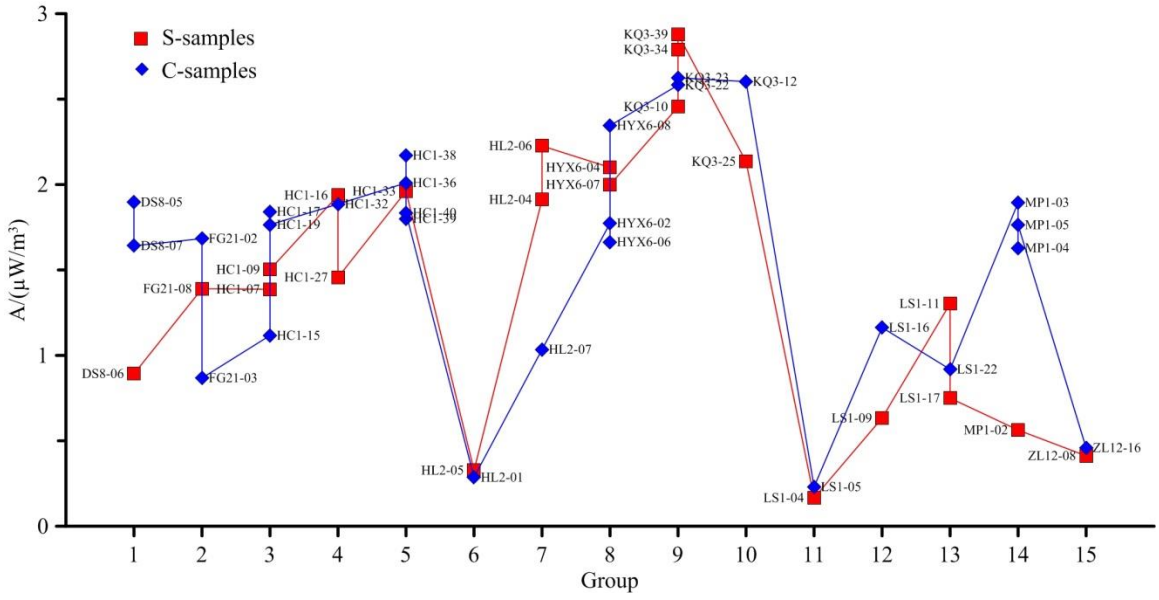

Fig. 2 Comparison of the heat production rate values of the S-group (analyzed by ICP-MS and ICP-OES) and C-group (analyzed by γ-ray spectrometry) samples

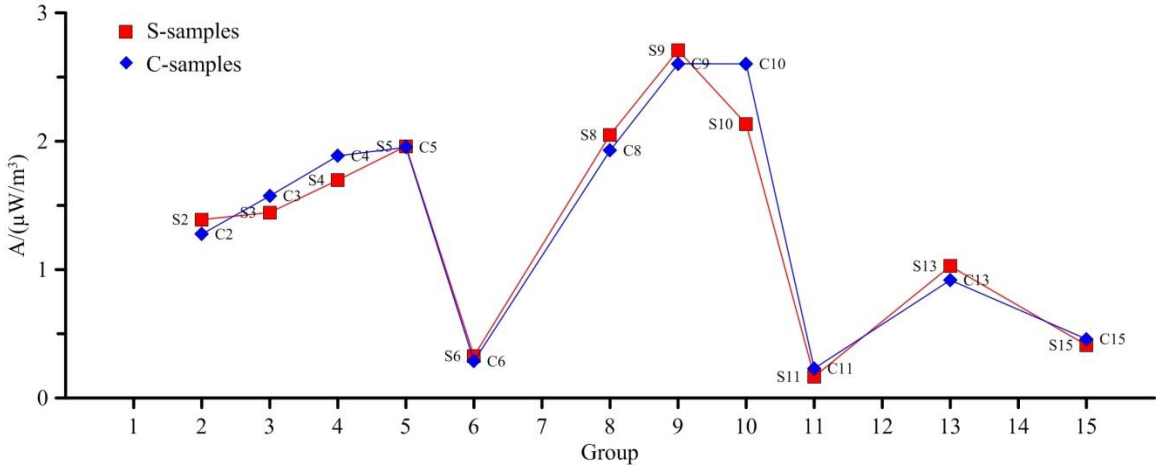

Fig. 3 Comparison of the average heat production rate values of the more consistent S-group (analyzed by ICP-MS and ICP-OES) and C-group (analyzed by γ-ray spectrometry) samples.

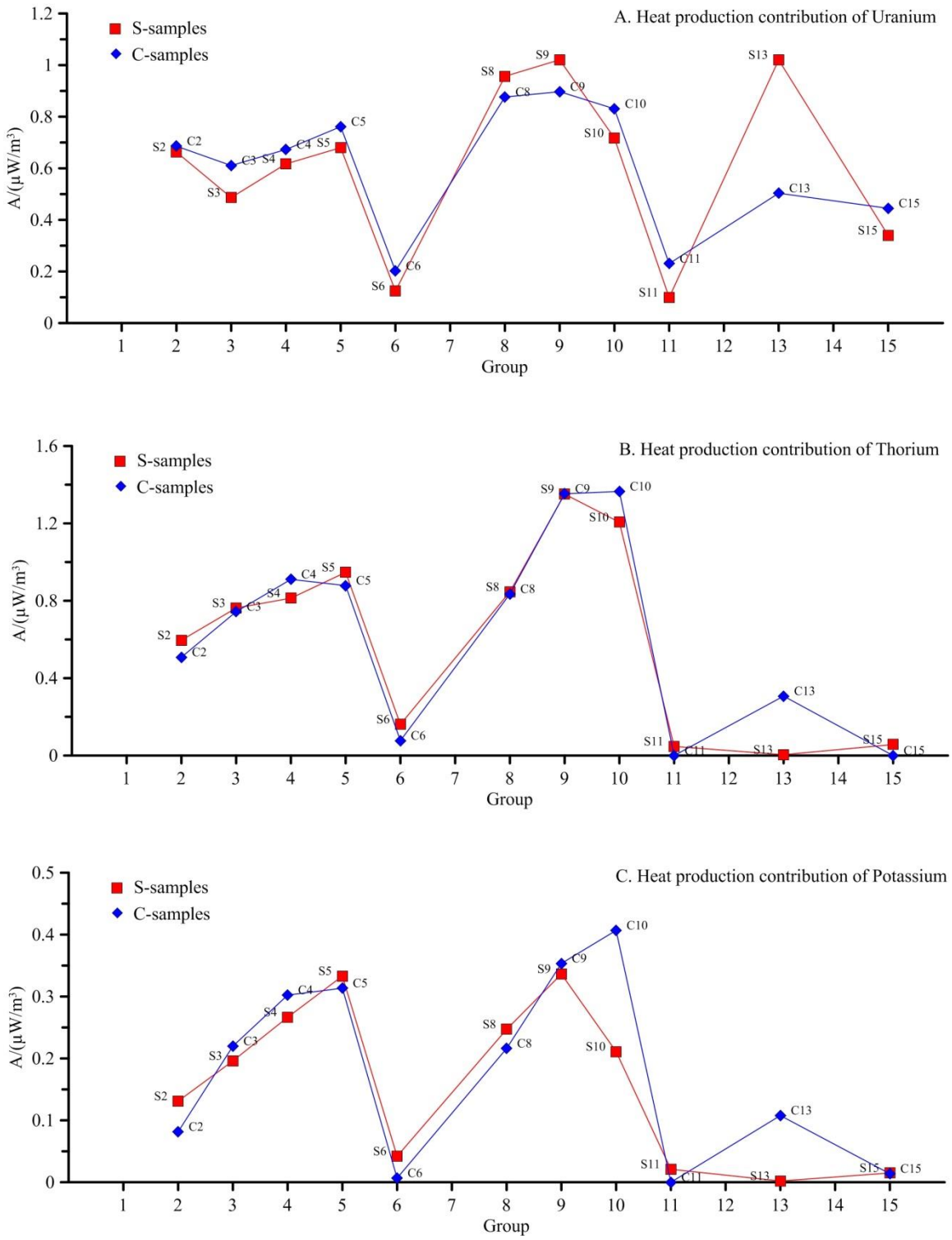

Fig. 4 Heat production rate contribution of radioactive heat-producing elements in the selected S-group (analyzed by ICP-MS and ICP-OES) and C-group (analyzed by γ-ray spectrometry) samples

281

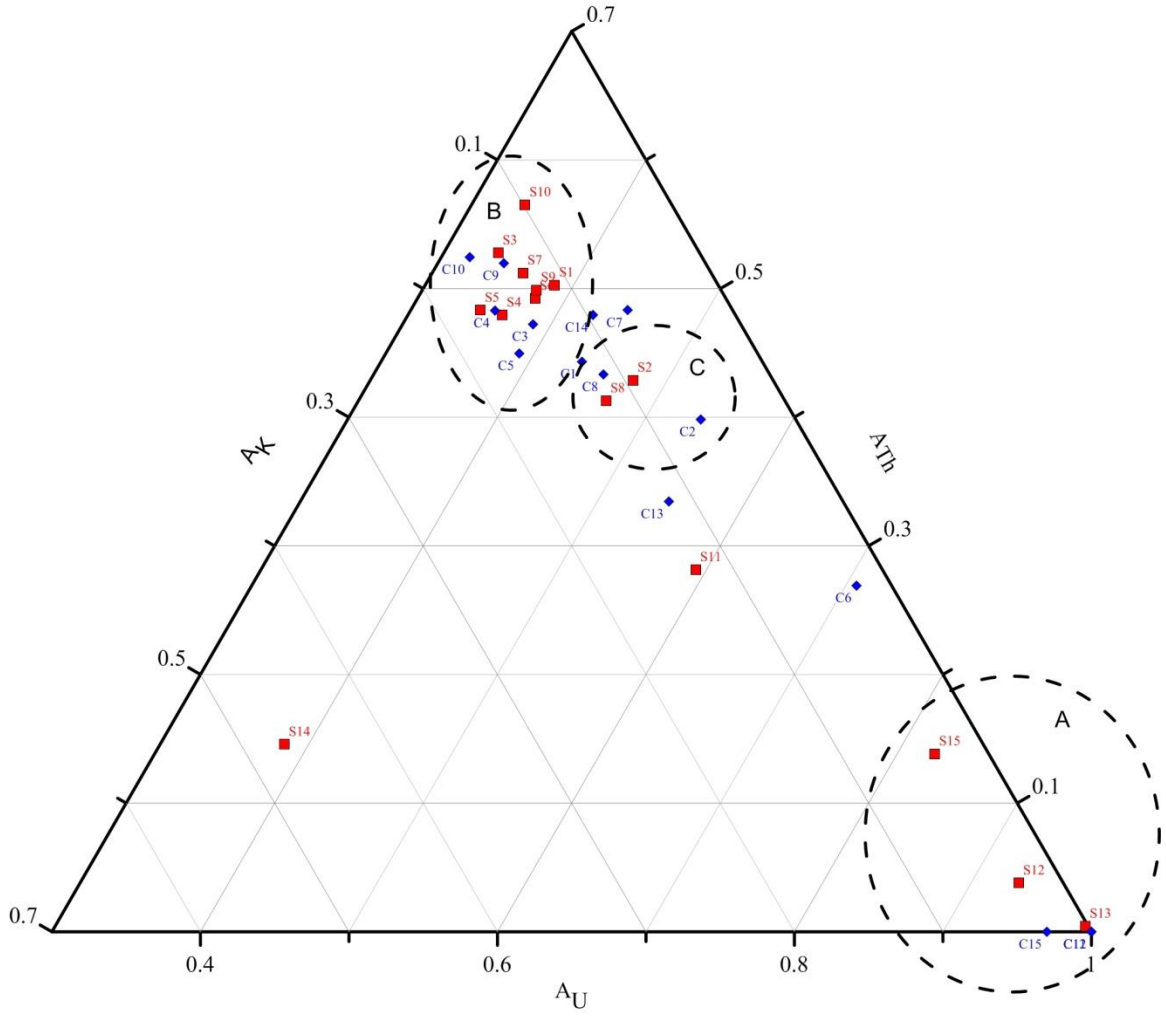

282

283 **Fig. 5** Ternary diagram of heat production rates of radioactive elements in samples

284

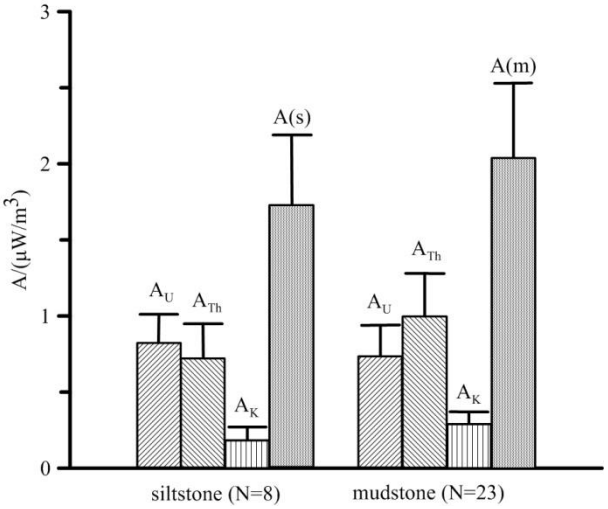

Fig. 6 Comparison of heat production rates and heat production contributions of various elements in siltstone and mudstone

Tables

Table 1 Sample information: S-samples measured using ICP-MS and ICP-OES, C-samples measured using γ-ray spectrometry

Group No.	Borehole	Strata	Lithology	Sample No.	Sampling code	Depth/m
G1	DS8	J_2s	sandstone	S1	DS8-06	2416.67
				C1	DS8-05	2642.69
					DS8-07	2517.26
G2	FG21	T_3x	siltstone	S2	FG21-08	3747.28
				C2	FG21-02	3785.74
					FG21-03	3784.64
G3	HC1	T_2zg	mudstone	S3	HC1-07	5844.5
					HC1-09	4776.8
				C3	HC1-15	4943.61
					HC1-17	4776.8
					HC1-19	4372.83
G4	HC1	T_3z	sandstone	S4	HC1-16	3784.5
					HC1-27	2268.8
				C4	HC1-32	3783.4
G5	HC1	T_3z	mudstone	S5	HC1-33	1316.27
				C5	HC1-36	3568.5
					HC1-38	3565.8
					HC1-39	3321.4
					HC1-40	3320.3
G6	HL2	J_1z	shell limestone	S6	HL2-05	2736.75
				C6	HL2-01	2746.2
G7	HL2	J_1z	shale	S7	HL2-04	2734.96
					HL2-06	2728.87
				C7	HL2-07	2734.96
G8	HYX6	K	siltstone	S8	HYX6-04	989.9
					HYX6-07	893.5
				C8	HYX6-02	1106.71
					HYX6-06	1013.38
					HYX6-08	988.8
G9	KQ3	$S_{1\text{-}2}wx$	mudstone	S9	KQ3-10	432.36
					KQ3-34	336.8
					KQ3-39	114.36
				C9	KQ3-22	422.89
					KQ3-23	421.79
G10	KQ3	$S_{1\text{-}2}wx$	lime mudstone	S10	KQ3-25	377.08
				C10	KQ3-12	438.56
G11	LS1	T_1j	dolomite	S11	LS1-04	6942.62
				C11	LS1-05	6946.93
G12	LS1	T_2l	dolarenite	S12	LS1-09	6512.76
				C12	LS1-16	6013.26
G13	LS1	T_2l	algae dolomite	S13	LS1-11	6323.11
					LS1-17	5993.37

				C13	LS1-22	6312.55
G14	MP1	J_3p	mudstone	S14	MP1-02	1364.4
				C14	MP1-03	1365.5
					MP1-04	1367.8
					MP1-05	1368.9
G15	ZL12	T_2l	dolomite	S15	ZL12-08	1332.43
				C15	ZL12-16	1331.33

293

Table 2 The calculated values for radioactive heat-producing element content and sample heat production rates using ICP-MS and ICP-OES*

Sample No.	Sampling code	ρ (g/cm^3)	U (μg/g)	Th (μg/g)	K (%)	A_U ($\mu W/m^3$)	A_{Th} ($\mu W/m^3$)	A_K ($\mu W/m^3$)	A_0 ($\mu W/m^3$)	A_S ($\mu W/m^3$)
S1	DS8-06	2.61	1.39±0.07	6.71±0.34	1.08±0.05	0.35±0.01	0.45±0.01	0.10±0.00	0.89±0.02	0.89
S2	FG21-08	2.70	2.58±0.13	8.62±0.43	1.39±0.07	0.66±0.01	0.60±0.01	0.13±0.00	1.39±0.03	1.39
S3	HC1-07	2.68	1.74±0.09	11.10±0.56	1.95±0.10	0.44±0.01	0.76±0.01	0.18±0.00	1.39±0.03	1.44
	HC1-09	2.71	2.05±0.10	11.00±0.55	2.22±0.11	0.53±0.01	0.76±0.01	0.21±0.00	1.50±0.03	
S4	HC1-16	2.57	2.66±0.13	14.50±0.72	3.71±0.19	0.65±0.01	0.95±0.02	0.33±0.01	1.94±0.04	1.70
	HC1-27	2.70	2.27±0.11	9.73±0.49	2.14±0.11	0.58±0.01	0.67±0.01	0.20±0.00	1.46±0.03	
S5	HC1-33	2.57	2.78±0.14	14.40±0.72	3.73±0.19	0.68±0.01	0.95±0.02	0.33±0.01	1.96±0.04	1.96
S6	HL2-05	2.69	0.48±0.05	2.34±0.12	0.45±0.02	0.12±0.01	0.16±0.00	0.04±0.00	0.33±0.01	0.33
S7	HL2-04	2.81	2.85±0.14	13.20±0.66	2.05±0.10	0.76±0.01	0.95±0.02	0.20±0.00	1.91±0.03	2.07
	HL2-06	2.72	2.83±0.14	16.80±0.84	3.42±0.17	0.73±0.01	1.17±0.02	0.32±0.01	2.23±0.04	
S8	HYX6-04	2.69	3.36±0.17	13.90±0.70	3.02±0.15	0.86±0.02	0.96±0.02	0.28±0.01	2.10±0.04	2.05
	HYX6-07	2.71	4.08±0.20	10.60±0.53	2.24±0.11	1.05±0.02	0.74±0.01	0.21±0.00	2.00±0.04	
S9	KQ3-10	2.74	3.01±0.15	18.20±1.82	4.13±0.21	0.79±0.01	1.28±0.05	0.39±0.01	2.46±0.07	2.71
	KQ3-34	2.79	4.98±0.25	17.50±0.88	2.24±0.11	1.32±0.02	1.25±0.02	0.22±0.00	2.79±0.05	
	KQ3-39	2.80	3.58±0.18	21.30±1.06	4.08±0.20	0.95±0.02	1.53±0.03	0.40±0.01	2.88±0.05	
S10	KQ3-25	2.77	2.72±0.14	17.00±1.70	2.19±0.11	0.72±0.01	1.21±0.04	0.21±0.00	2.13±0.06	2.13
S11	LS1-04	2.74	0.38±0.04	0.67±0.07	0.22±0.01	0.10±0.01	0.05±0.01	0.02±0.00	0.17±0.02	0.17
S12	LS1-09	2.67	2.32±0.12	0.36±0.04	0.20±0.02	0.59±0.01	0.02±0.00	0.02±0.00	0.63±0.01	0.63
S13	LS1-11	2.74	4.96±0.25	0.09±0.01	0.03±0.00	1.29±0.02	0.01±0.00	0.00±0.00	1.30±0.02	1.03
	LS1-17	2.75	2.85±0.14	0.04±0.00	0.01±0.00	0.75±0.01	0.00±0.00	0.00±0.00	0.75±0.01	
S14	MP1-02	2.65	0.86±0.09	1.21±0.06	2.87±0.14	0.22±0.01	0.08±0.00	0.27±0.01	0.56±0.02	0.56
S15	ZL12-08	2.86	1.25±0.06	0.781±0.08	0.15±0.02	0.34±0.01	0.06±0.00	0.02±0.00	0.41±0.01	0.41

*__Notes__: The data was analyzed at the Beijing Research Institute of Uranium Geology, while the experiment was run according to the QC reference material GBW07106. The blank values of both U and Th were adopted as 0.003ng/ml. The relative standard deviation (RSD) of the individual data was given by estimated as: RSD<5%, while the concentration > 1ppm; RSD<10%, while the concentration < 1ppm.

Table 3 The calculated values for radioactive heat-producing element content and sample heat production rates using gamma-ray spectrometry*

Sample No.	Sampling code	ρ (g/cm^3)	^{238}U (dpm/g)	^{238}U (μg/g)	^{232}Th (dpm/g)	^{232}Th (μg/g)	^{40}K (dpm/g)	^{40}K (%)	A_U ($\mu W/m^3$)	A_{Th} ($\mu W/m^3$)	A_K ($\mu W/m^3$)	A_0 ($\mu W/m^3$)	A_C ($\mu W/m^3$)
C1	DS8-05	2.63	2.29±0.05	3.07±0.06	3.09±0.03	12.67±0.14	54.82±0.88	3.01±0.05	0.77±0.01	0.85±0.00	0.28±0.00	1.90±0.01	1.77
	DS8-07	2.63	2.30±0.05	3.08±0.07	2.59±0.04	10.63±0.16	30.67±0.83	1.69±0.05	0.77±0.01	0.72±0.00	0.16±0.00	1.64±0.01	
C2	FG21-02	2.63	2.26±0.05	3.03±0.07	2.85±0.04	11.70±0.16	27.34±0.78	1.50±0.04	0.76±0.01	0.79±0.00	0.14±0.00	1.68±0.01	1.28
	FG21-03	2.65	1.81±0.05	2.43±0.06	0.82±0.02	3.37±0.10	5.02±0.47	0.28±0.03	0.61±0.01	0.23±0.00	0.03±0.00	0.87±0.01	
C3	HC1-15	2.85	1.23±0.05	1.65±0.07	1.76±0.04	7.21±0.15	26.16±0.89	1.44±0.05	0.45±0.01	0.53±0.00	0.14±0.00	1.12±0.01	1.57
	HC1-17	2.67	1.86±0.05	2.49±0.07	3.30±0.05	13.54±0.19	55.21±1.13	3.04±0.06	0.63±0.01	0.93±0.01	0.28±0.00	1.84±0.01	
C4	HC1-19	2.76	2.13±0.05	2.86±0.06	2.69±0.04	11.03±0.15	44.41±0.90	2.44±0.05	0.75±0.01	0.78±0.00	0.23±0.00	1.77±0.01	1.89
	HC1-32	2.57	2.06±0.05	2.75±0.07	3.37±0.04	13.84±0.17	61.42±1.08	3.38±0.06	0.67±0.01	0.91±0.00	0.30±0.00	1.89±0.01	
C5	HC1-36	2.85	1.97±0.05	2.63±0.07	3.11±0.04	12.76±0.18	67.00±1.20	3.68±0.07	0.71±0.01	0.93±0.01	0.37±0.00	2.01±0.01	1.95
	HC1-38	2.77	2.26±0.05	3.03±0.07	3.53±0.04	14.50±0.18	64.69±1.11	3.56±0.06	0.80±0.01	1.03±0.01	0.34±0.00	2.17±0.01	
	HC1-39	2.77	2.14±0.05	2.87±0.07	2.50±0.04	10.26±0.16	59.54±1.07	3.27±0.06	0.76±0.01	0.73±0.00	0.32±0.00	1.80±0.01	
	HC1-40	2.87	2.12±0.05	2.84±0.07	2.74±0.04	11.26±0.17	42.09±0.97	2.31±0.05	0.78±0.01	0.83±0.00	0.23±0.00	1.83±0.01	
C6	HL2-01	2.76	0.58±0.03	0.77±0.04	0.26±0.02	1.09±0.07	1.27±0.34	0.07±0.02	0.20±0.00	0.08±0.00	0.01±0.00	0.29±0.01	0.29
C7	HL2-07	2.77	1.30±0.04	1.75±0.05	1.72±0.03	7.05±0.12	13.81±0.59	0.76±0.03	0.46±0.01	0.50±0.00	0.07±0.00	1.04±0.01	1.04
C8	HYX6-02	2.89	2.02±0.04	2.70±0.06	2.80±0.04	11.49±0.15	32.72±0.78	1.80±0.04	0.74±0.01	0.85±0.00	0.18±0.00	1.77±0.01	1.93
	HYX6-06	2.71	2.16±0.04	2.89±0.06	2.62±0.03	10.76±0.13	33.16±0.71	1.82±0.04	0.75±0.01	0.75±0.00	0.17±0.00	1.66±0.01	
	HYX6-08	2.68	3.34±0.06	4.47±0.08	3.23±0.04	13.25±0.18	57.72±1.10	3.17±0.06	1.14±0.01	0.91±0.01	0.30±0.00	2.35±0.01	
C9	KQ3-22	2.77	2.77±0.05	3.71±0.07	4.41±0.04	18.12±0.18	60.13±1.00	3.31±0.06	0.98±0.01	1.29±0.01	0.32±0.00	2.58±0.01	2.60
	KQ3-23	2.8	2.29±0.05	3.06±0.07	4.83±0.05	19.83±0.20	72.39±1.17	3.98±0.06	0.82±0.01	1.42±0.01	0.39±0.00	2.63±0.01	
C10	KQ3-12	2.77	2.35±0.05	3.15±0.07	4.69±0.05	19.25±0.19	76.72±1.13	4.22±0.06	0.83±0.01	1.37±0.01	0.41±0.00	2.60±0.01	2.60
C11	LS1-05	2.72	0.67±0.07	0.89±0.06	—	—	—	—	0.23±0.01	—	—	0.23±0.01	0.23
C12	LS1-16	2.77	3.29±0.04	4.41±0.06	—	—	—	—	1.16±0.01	—	—	1.16±0.01	1.16
C13	LS1-22	2.74	1.44±0.06	1.93±0.08	1.07±0.04	4.38±0.15	20.63±0.92	1.13±0.05	0.50±0.01	0.31±0.00	0.11±0.00	0.92±0.01	0.92
C14	MP1-03	2.65	2.23±0.02	2.99±0.03	3.28±0.03	13.48±0.12	44.56±0.91	2.45±0.05	0.75±0.00	0.91±0.00	0.23±0.00	1.90±0.01	1.76
	MP1-04	2.56	2.33±0.06	3.12±0.08	2.86±0.05	11.75±0.19	19.98±0.83	1.10±0.05	0.76±0.01	0.77±0.01	0.10±0.00	1.63±0.01	
	MP1-05	2.76	2.08±0.04	2.78±0.06	2.93±0.03	12.04±0.14	34.63±0.71	1.90±0.04	0.73±0.01	0.85±0.00	0.18±0.00	1.76±0.01	
C15	ZL12-16	2.64	1.32±0.04	1.77±0.05	—	—	2.71±0.37	0.15±0.02	0.44±0.01	—	0.01±0.00	0.46±0.01	0.46

***Notes:** The measurements of the radioactivity concentrations were carried out at the Lab of Cosmogenic Nuclide Chronology, Institute of Geology and Geophysics, Chinese Academy of Sciences, according to the QC standard GBW08304. Dpm/g is the radioactivity specific activity (unit: the number of decayed atoms per gram of sample per minute). σ is the standard deviation (unit: dpm/g = 1/60 Bq/g). "—" indicates sample radioactivity below the minimum detection limit when the calculation value is "0". Content calculation principle is the number of decayed atoms per second in a radioactive element or isotope (radioactivity specific activity is the radioactivity of a nuclide per unit mass of material), expressed by the formula $A=\lambda N$ where A is radioactivity specific activity, λ is the decay constant ($\lambda = \ln 2/T$, where T is the half-life of a nuclide) and N is the number of decayed nuclides in a unit of mass. For details on the method of obtaining the nuclide content of a material based on radioactive specific activity could be found from references [16-21]. A_U, A_{Th}, A_K indicates the heat-production rate of the U, Th and K respectively, while A_C indicates the heat-production rate of each S-sample.

References

1. Kramers JD, Kreissig K, Jones MQ (2001) Crustal heat production and style of metamorphism: a comparison between two Archean high grade provinces in the Limpopo Belt, southern Africa. Precambrian Res 112: 149-163
2. He LJ, Hu SB, Yang WC, Wang JY (2009) Radiogenic heat production in the lithosphere of Sulu ultrahigh-pressure metamorphic belt. Earth Planet Sc Lett 277: 525-538
3. Verdoya M, Pasquale V, Chiozzi P, Kukkonen IT (1998) Radiogenic heat production in the Variscan crust: new determinations and distribution models in Corsica (northwestern Mediterranean). Tectonophysics 291: 63-75
4. Rudnick RL, McDonough WF, O'Connell RJ (1998) Thermal structure, thickness and composition of continental lithosphere. Chem Geol 145: 395-411
5. Kumar PS, Reddy GK (2004) Radioelements and heat production of an exposed Archaean crustal cross-section, Dharwar craton, south India. Earth Planet Sc Lett 224: 309-324
6. Kumar PS, Menon R, Reddy GK (2009) Heat production heterogeneity of the Indian crust beneath the Himalaya: Insights from the northern Indian Shield. Earth Planet Sc Lett 283: 190-196
7. Hasterok D, Chapman DS (2011) Heat production and geotherms for the continental lithosphere. Earth Planet Sc Lett 307: 59-70
8. Yamaguchi TI, Yamano M, Nagao T, Goto S (2001) Distribution of radioactive heat production around an active fault and in accretionary prisms of southwest Japan. Phys Earth Planet In 126: 269-277
9. Kumar PS, Menon R, Reddy GK (2007) The role of radiogenic heat production in the thermal evolution of a Proterozoic granulite-facies orogenic belt: Eastern Ghats, Indian Shield. Earth Planet Sc Lett 254: 39-54
10. Artemieva IM, Mooney WD (2001) Thermal thickness and evolution of Precambrian lithosphere: a global study. J Geophys Res-Sol Ea 106: 16387-16414
11. Hasterok D, Chapman DS (2007) Continental thermal isostasy: 1. Methods and sensitivity. J Geophys Res-Sol Ea 112: B06414

12. Brady RJ, Ducea MN, Kidder SB, Saleeby JB (2006) The distribution of radiogenic heat production as a function of depth in the Sierra Nevada Batholith, California. Lithos 86: 229-244
13. Ketcham RA (1996) An improved method for determination of heat production with γ-ray scintillation spectrometry. Chem Geol 130: 175-194
14. Chiozzi P, De Felice P, Fazio A, Pasquale V, Verdoya M (2000) Laboratory application of NaI (Tl) γ-ray spectrometry to studies of natural radioactivity in geophysics. Appl Radiat Isotopes 53: 127-132
15. Tzortzis M, Tsertos H, Christofides S, Christodoulides G (2003) γ-ray measurements of naturally occurring radioactive samples from Cyprus characteristic geological rocks. Radiat Meas 37: 221-229
16. Abbady AG, El-Arabi AM, Abbady A (2006) Heat production rate from radioactive elements in igneous and metamorphic rocks in Eastern Desert, Egypt. Appl Radiat Isotopes 64:131-137
17. Abbady A (2006) Radiological hazard and radiogenic heat production in some building materials in upper Egypt. J Radioanal Nucl Ch 268: 243-246
18. Xhixha G, Bezzon GP, Broggini C, Buso GP, Caciolli A, Callegari I, Bianchi SD, Fiorentini G, Guastaldi E, Xhixha MK, Mantovani F, Massa G, Menegazzo R, Mou L, Pasquini A, Alvarez CR, Shyti M (2013) The worldwide NORM production and a fully automated γ-ray spectrometer for their characterization. J Radioanal Nucl Ch 295: 445-457
19. Ibrahim N (1999) Natural activities of 238U, 232Th and 40K in building materials. J Environ Radioactiv, 43: 255-258
20. Foster IDL, Boardman J, Keay-Bright J, Meadows ME (2005) Land degradation and sediment dynamics in the South African Karoo. International Association of Hydrological Sciences Publication, 292, 207-213
21. Hamby DM, Tynybekov AK (2000) Uranium, thorium and potassium in soils along the shore of lake Issyk-Kyol in the Kyrghyz RepublicEnviron. Monit. Assess, 73, 101-108.
22. Fiorentini G, Lissia M, Mantovani F (2007) Geo-neutrinos and earth's interior. Phys Rep 453: 117-172

62 23. Enomoto S, Ohtani E, Inoue K, Suzuki A (2007) Neutrino geophysics with
63 KamLAND and future prospects. Earth Planet Sc Lett 258: 147-159
64 24. Dye S (2011) Geo-neutrinos as indicators of the origin and thermal history of the
65 Earth. Rev Geophys 5(arXiv: 1111.6099), 0.
66 25. Rybach L (1988) In: Hänel L, Rybach L, Stegena L (Eds) Handbook of Terrestrial
67 Heat Flow Density Determination. Kluwer, Dordrecht.
68 26. Xhixha M (2014) New γ-ray spectrometry methods for estimating K, U, Th
69 concentrations in rocks of the Sardinia Batholith. University Of Sassari
70 27. Qiu NS (2003) Geothermal regime in the Qaidam basin, northeast Qinghai-Tibet
71 Plateau. Geol Mag 140: 707-719
72 28. Chiozzi P, Pasquale V, Verdoya M (2002) Naturally occurring radioactivity at the
73 Alps–Apennines transition. Radiat Meas 35: 147-154
74 29. Pasquale V, Verdoya M, Chiozzi P (2001) Radioactive heat generation and its
75 thermal effects in the Alps–Apennines boundary zone. Tectonophysics 331: 269-283
76 30. Abbady AG (2010) Evaluation of heat generation by radioactive decay of
77 sedimentary rocks in Eastern Desert and Nile Valley, Egypt. Appl Radiat Isotopes
78 68: 2020-2024
79 31. Čermák V, Haenel R (1982) Geothermics and geothermal energy. Schweizerbart
80 Science Publishers, Schweizerbart
81 32. Čermák V (1982) Crustal temperature and mantle heat flow in Europe.
82 Tectonophysics 83: 123-142
83 33. Roque A, Ribeiro FB (1997) Radioactivity and radiogenic heat production in the
84 sediments of the São Francisco sedimentary basin, Central Brazil. Appl Radiat
85 Isotopes 48: 413-422
86 34. Ribeiro FB, Roque A (2001) Vertical distributions of uranium, thorium and
87 potassium and of volumetric heat production rates in the sediments of the São
88 Francisco basin, Central Brazil. Appl Radiat Isotopes 55: 393-405
89 35. Vilà M, Fernández M, Jiménez-Munt I (2010) Radiogenic heat production variability
90 of some common lithological groups and its significance to lithospheric thermal
91 modeling. Tectonophysics 490: 152-164

36. Murthy VR, Van Westrenen W, Fei Y (2003) Experimental evidence that potassium is a substantial radioactive heat source in planetary cores. Nature 423: 163-165